CONDENSED MATTER PHYSICS

10.1126/sciadv.1501329

Quantitative determination of pairing interactions for high-temperature superconductivity in cuprates

Jin Mo Bok,[1,2] Jong Ju Bae,[1] Han-Yong Choi,[1,3]* Chandra M. Varma,[4]* Wentao Zhang,[2,5] Junfeng He,[2] Yuxiao Zhang,[2] Li Yu,[2] X. J. Zhou[2,6]*

A profound problem in modern condensed matter physics is discovering and understanding the nature of fluctuations and their coupling to fermions in cuprates, which lead to high-temperature superconductivity and the invariably associated strange metal state. We report the quantitative determination of normal and pairing self-energies, made possible by laser-based angle-resolved photoemission measurements of unprecedented accuracy and stability. Through a precise inversion procedure, both the effective interactions in the attractive d-wave symmetry and the repulsive part in the full symmetry are determined. The latter is nearly angle-independent. Near T_c, both interactions are nearly independent of frequency and have almost the same magnitude over the complete energy range of up to about 0.4 eV, except for a low-energy feature at around 50 meV that is present only in the repulsive part, which has less than 10% of the total spectral weight. Well below T_c, they both change similarly, with superconductivity-induced features at low energies. Besides finding the pairing self-energy and the attractive interactions for the first time, these results expose the central paradox of the problem of high T_c: how the same frequency-independent fluctuations can dominantly scatter at angles $\pm\pi/2$ in the attractive channel to give d-wave pairing and lead to angle-independent repulsive scattering. The experimental results are compared with available theoretical calculations based on antiferromagnetic fluctuations, the Hubbard model, and quantum-critical fluctuations of the loop-current order.

INTRODUCTION

Quantitative analysis of very precise tunneling experiments, conducted by McMillan and Rowell (*1*) using the Eliashberg theory (*2*, *3*), decisively confirmed that the exchange of phonons with fermions is responsible for the conventional s-wave pairing in metals such as Pb. Tunneling experiments integrate over the momentum dependence of many-body effects. This is sufficient for s-wave superconductors because the normal and superconducting properties have the full symmetry of the lattice. For any superconductor, the dependence of the normal self-energy $\Sigma(\mathbf{k}, \omega)$ on the momentum $\mathbf{k}$ has the full symmetry of the lattice; however, for high-temperature superconductors such as cuprates, the dependence of the pairing self-energy $\phi(\mathbf{k}, \omega)$ on $\mathbf{k}$ has a B_{1g} or $d_{x^2-y^2}$ symmetry. Correspondingly, the effective interaction spectrum is characterized by two functions—(i) with the full symmetry of the lattice, which we will call the normal Eliashberg function $\varepsilon_N(\mathbf{k}, \omega)$, and (ii) with the pairing symmetry, which we will call the pairing Eliashberg function $\varepsilon_P(\mathbf{k}, \omega)$ —rather than by a single function sufficient for s-wave pairing, which is often denoted by $\alpha^2F(\omega)$ (*1*). The much more sophisticated angle-resolved photoemission spectroscopy (ARPES) experiments (*4*, *5*) are then required because both the momentum dependence and the frequency dependence of the interactions are necessary to decipher the fundamental physics. The procedure used for determining fluctuations using the Eliashberg theory remains valid for the pairing mediated by collective fluctuations, even when their high-energy cutoff is comparable to the electronic bandwidth.

RESULTS OF ARPES EXPERIMENTS

The procedure for extracting normal and pairing self-energies is described in section SI. The conditions required for ARPES to quantitatively yield the electron self-energies are very demanding. We seek to measure the absolute magnitude of the photoelectron current per unit-photon flux at various temperatures above and below T_c, at various angles, and across a range of frequencies extending to the upper cutoff of the fluctuations. Requirements on the data, estimates of signal-to-noise errors and systematic errors, partial correction of systematic errors, and limits of the validity of our results and analysis are given in section SII.

We carried out high-resolution laser-ARPES measurements on two $Bi_2Sr_2CaCu_2O_{8+\delta}$ (Bi2212) samples—one slightly underdoped with a T_c of 89 K (UD89 hereafter) and the other overdoped with a T_c of 82 K (OD82 hereafter)—along various momentum cuts and at various temperatures. Some of the data on UD89 (*6*) and OD82 (*7*) (only for energy $\lesssim$0.1 eV below T_c) were reported earlier, but without the analysis (and extension to higher energy) essential for deciphering the physics, as presented in this work. Figure 1 shows an example of the measured data of photoemission intensity as a function of momentum and energy, along a momentum cut marked in the inset to Fig. 1B, at temperatures well below T_c (Fig. 1A) and above T_c (Fig. 1B) in the UD89 sample. As shown in Fig. 1C, the data at different temperatures overlap each other at high binding energies extremely well, showing

[1]Department of Physics and Institute for Basic Science Research, SungKyunKwan University, Suwon 440-746, Korea. [2]National Laboratory for Superconductivity, Beijing National Laboratory for Condensed Matter Physics, Institute of Physics, Chinese Academy of Sciences, Beijing 100190, China. [3]Asia Pacific Center for Theoretical Physics, Pohang 790-784, Korea. [4]Department of Physics and Astronomy, University of California, Riverside, CA 92521, USA. [5]Department of Physics and Astronomy, Shanghai JiaoTong University, Shanghai 200240, China. [6]Collaborative Innovation Center of Quantum Matter, Beijing 100871, China.
*Corresponding author. E-mail: hychoi@skku.ac.kr (H.-Y.C.); chandra.varma@ucr.edu (C.M.V.); xjzhou@aphy.iphy.ac.cn (X.J.Z.)

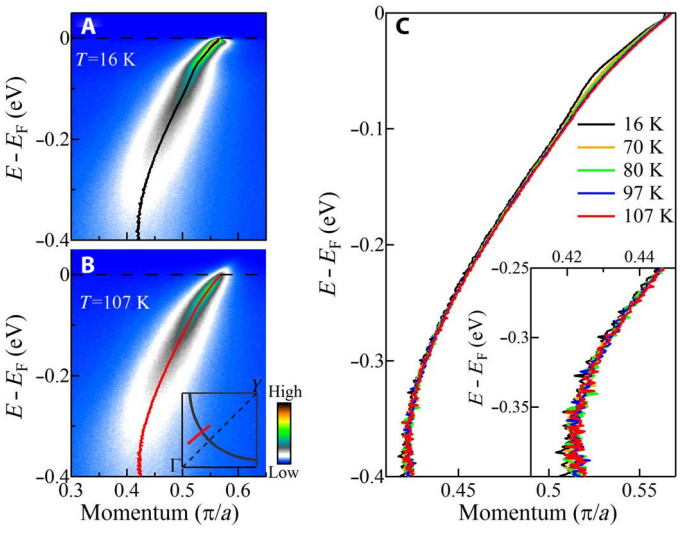

Fig. 1. Color representation of the measured photoemission intensity of the UD89 sample along the θ = 35° direction. (**A**) $T = 16$ K. (**B**) $T = 107$ K. (**C**) Progression of energy-momentum dispersions at temperatures of 16, 70, 80, 97, and 107 K. The inset to (C) presents, on an expanded scale, an illustration of the consistency of the data up to an accuracy of $5 \times 10^{-3}(\pi/a)$ in the region at high energy where no temperature-dependent corrections to the dispersion are necessary. In section SII, we show the systematic errors in the data when such accuracy is not met and how we correct them.

their high quality and reproducibility. For some momentum cuts where the dispersions show small drifts with temperature and for other systematic errors, we used a method of data correction (section SII).

The suggested strategy (*8*) for extracting many-body effects relies on momentum distribution curves (MDCs), which represent the intensity of photoelectrons as a function of momentum $k_\perp$ perpendicular to the Fermi surface for various fixed energies (for example, across the horizontal cuts in Fig. 1A or Fig. 1B). The two-dimensional momentum **k** is represented by the angle θ with respect to the crystalline axis and the magnitude $k_\perp$ measured from the $(\pi/a, \pi/a)$ point, as shown in Fig. 2C. In Fig. 2A, we present the measured MDC for UD89 for one of the trajectories across the Fermi surface at five energies ω in the normal state above T_c (red circles) and in the superconducting state at 16 K (blue circles). These MDCs are from more than 5000 such plots taken; the results presented here are derived from the analysis of such plots in the two samples at various temperatures, angles, and energies. The signal-to-noise ratio of the fit in Fig. 2A may be best appreciated in Fig. 2B, where the normalized difference in the measured MDC intensities between 16 and 97 K is compared to the same function calculated from the fits in Fig. 2A. This represents the best results we have obtained; acceptable results are shown for the OD82 sample in fig. S1.

NORMAL AND PAIRING SELF-ENERGIES

The relation of the measured photoelectron intensity $I(\mathbf{k}, \omega)$ to the spectral function $A(\mathbf{k}, \omega)$ is described in the Supplementary Materials, where we also present the procedure for extracting the normal self-energy $\Sigma(\mathbf{k}, \omega)$ and the pairing self-energy $\phi(\mathbf{k}, \omega)$ by fitting the MDCs. Representative fits are shown in Fig. 2A. The MDCs in the normal state in Fig. 2A (red circles) over a wide region of energy and momentum are very well represented by Lorentzians as a function of $k_\perp$. This is true precisely (*9*) only if $\Sigma(\mathbf{k}, \omega)$ is a function only of θ and ω. In the superconducting state, we fit the MDCs with $\phi(\mathbf{k}, \omega)$ depending only on θ and ω, with almost equally good results, as shown in Fig. 2A (blue circles). As a further measure of confidence in the data and determination of the self-energies, we compare the measured photoemission spectrum [energy distribution curve (EDC)] at a fixed momentum to the EDC calculated from our fit to the MDCs at various energies in Fig. 2D.

We present the self-energies obtained directly from such fits in Fig. 3 so that the signal-to-noise ratio and the limits on the consistency of the data are directly visible. The evolution of the magnitude of the extracted normal and pairing self-energies is shown as a function of energy at various temperatures in Fig. 3 (A and B, respectively) for θ = 20° in OD82. The pairing self-energy measured at various θ at a temperature of 16 K for the UD89 sample is shown in Fig. 3C. Note that $\phi(\theta, \omega)$ has been scaled by $\cos(2\theta)$. Within the uncertainties in the data, the conclusions are the same if we scale instead by the appropriate d-wave basis for a square lattice $[\cos(k_x a/\pi) - \cos(k_y a/\pi)]$.

The self-energies near T_c are sufficient to deduce the effective interactions leading to the value of T_c. Near T_c, the real and imaginary parts of both normal and pairing self-energies are smooth functions of energies up to high energies (and angles). However, as T decreases below T_c, one finds in Fig. 3 two low-energy features below ~75 meV. It was suggested (*10*) and experimentally shown (*11*) that forward scattering (*9*) from impurities lying in between the CuO_2 planes produces the low-energy peak at ~15 meV in the self-energies at the superconducting state. The other structure at about 65 meV is expected for all cases in which the fluctuations are due to the interactions among the fermions themselves (*12*, *13*) because the opening of the superconducting gap Δ diminishes the spectral weight at energies below $O(2\Delta)$ and piles it up at higher energies. This process occurs in addition to the generalization to d-wave superconductors of the shift of the self-energies by Δ, which is well known in phonon-mediated s-wave superconductors. These two superconductivity-induced features are irrelevant in determining the value of T_c, although they are quite important in determining the temperature dependence of the superconducting gap, which is not our focus in this paper.

In Fig. 3A, except for the low-energy features, the normal (real and imaginary) self-energy $\Sigma(\theta, \omega)$ is nearly independent of temperature. The imaginary part $\Sigma_2(\theta, \omega)$ varies linearly with ω to a good approximation, as in the normal state. In the same energy range, $\Sigma_2(\theta, \omega)$ is also nearly independent of θ, as already noted by Valla *et al.* (*14*), Kaminski *et al.* (*15*), and Bok *et al.* (*16*). On the other hand, not surprisingly, the real and imaginary parts of the pairing self-energy $\phi(\theta, \omega)$ in Fig. 3B systematically increase with decreasing temperature below T_c, with saturation at low temperatures. Except for the low-energy features, the imaginary part of $\phi(\theta, \omega)$ in Fig. 3B is weakly ω -dependent up to about 0.2 eV, beyond which the signal-to-noise level does not allow quantitative conclusions. In Fig. 3C, we show that the real and imaginary parts of the pairing self-energy $\phi(\theta, \omega)$ scaled by $\cos(2\theta)$ over the energy range up to ~0.2 eV are also independent of θ up to about ±10% in absolute value. This is an important check on data and analysis because, in these experiments, this is the quantity deduced with the largest error as it comes from the difference between the spectra below T_c and the spectra above T_c. At θ = 20°, the bottom of the band from the Fermi energy is ~0.2 eV (*17*), which serves as the

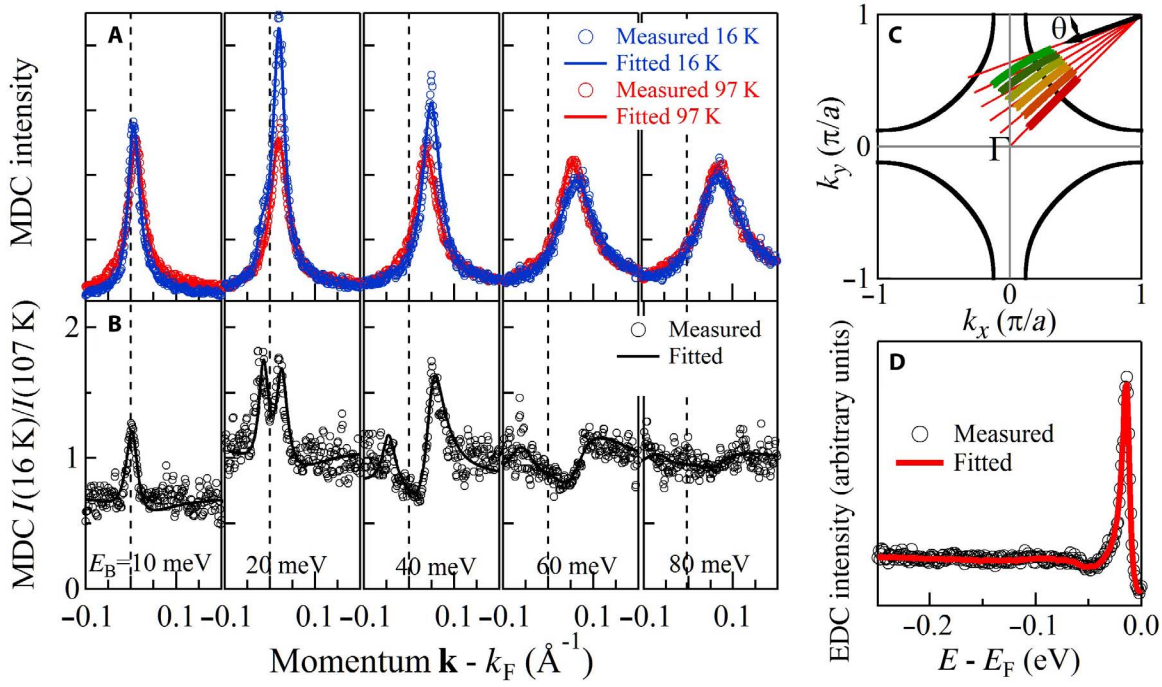

Fig. 2. Measured MDCs and their fits at five different energies at 97 and 16 K in the UD89 sample along the dark-green trajectory (θ = 20°). Such data were taken at 1-meV intervals and at all of the trajectories shown in (**C**). The vertical scale in (**A**) is the measured photoelectron current for a fixed photon flux (in arbitrary units). It is crucial that this scale remain within the error bars discussed in the text at all temperatures, energies, and momenta, and that any systematic errors be corrected. (**B**) Normalized difference in measurements taken at the two temperatures in (A) and at the same quantity calculated from the fits in (A). The fits to the MDCs were made according to the procedure described in fig. S1. The normal and pairing self-energies are extracted from such fits, also as described in fig. S1. (**D**) intends to show the consistency of the fits to the MDCs at different energies; it shows the EDC generated from the MDC within the complete range of energies measured at an angle θ = 20° at the Fermi surface at 16 K and compares direct measurements of the EDC at the same point and same temperature.

natural cutoff. Therefore, the complete fluctuation spectra have been accessed for this angle. From the measurements of $\Sigma(\theta, \omega)$ above T_c in Bok *et al.* (*16*) and below T_c found here, the cutoff energy increases smoothly with increasing θ (to ~0.4 eV for θ = 45°). It appears reasonable to assume that the pairing self-energy at other angles has the same cutoff as that of the normal self-energy, as it does at θ = 20°; this can be verified by future experiments with better signal-to-noise ratios for $\phi(\theta, \omega)$ at higher energies, θ values closer to 45°, and T values closer to T_c.

NORMAL AND PAIRING ELIASHBERG FUNCTIONS

Important conclusions about the fundamental physics of cuprates can already be reached from the self-energies (Fig. 3), which have been directly extracted from the experimental data. Reaching some other conclusions requires solving the Eliashberg integral equations for anisotropic superconductivity, described in section SIII. In section SIII, we show, using the experimentally obtained normal and pairing self-energies as inputs, that the determination of the Eliashberg functions $\varepsilon_N(\theta, \omega)$ and $\varepsilon_P(\theta, \omega)$ is limited only by the accuracy of the self-energies and by the procedure for solving the integral equations. We will also provide a self-consistency check on the validity of this procedure using the experimental results.

$\varepsilon_N(\theta, \omega)$ and $\varepsilon_P(\theta, \omega)$ are deduced from the measured self-energies $\Sigma(\theta, \omega)$ and $\phi(\theta, \omega)$ in Fig. 3 through solution of the integral equations using the maximum entropy method (*18*). To avoid instabilities in the numerical solutions of these equations using such a procedure, we smoothened the raw data of self-energies (such as those shown in Fig. 3, A to C) at each energy by averaging the data in the range of ±5 meV around it (as exemplified in Fig. 3D). The results obtained are shown in Fig. 4 for both UD89 and OD82. Despite the smoothening of self-energy, we found weak oscillations of about 10% magnitude in ε_N and ε_P, which are artifacts from the maximum entropy method. In Fig. 4, we plot $\varepsilon_N(\theta, \omega)$ and the scaled quantity $\varepsilon_P(\theta, \omega) \equiv \varepsilon_P(\theta, \omega)/\cos(2\theta)$.

Let us start with Fig. 4C, which presents results close to T_c. The normal-state bump at ~50 meV in $\varepsilon_N(\theta, \omega)$ hardly changes for $T \lesssim T_c$ and is absent in $\varepsilon_P(\theta, \omega)$. If we ignore the bump, $\varepsilon_P(\theta, \omega) \approx \varepsilon_N(\theta, \omega)$ to within 10% accuracy. As T decreases well below T_c, both functions develop a peak in the region around 50 to 75 meV, as shown in Fig. 4 (A and B). These are related to the superconductivity-induced features in the self-energies that we have already discussed. The result that $\varepsilon_P(\theta, \omega)$ loses the low-energy feature as $T \rightarrow T_c$ is highlighted in Fig. 4F, where its evolution with temperature is shown.

For comparison, we also include $\varepsilon_N(\theta, \omega)$, which was deduced from its self-energy in the normal state at various angles by the same methods used in Fig. 4 (D and E). These results are consistent with earlier deductions (*19*) from ARPES data along the diagonal (θ = 45°) direction, derived using the same technique and by fitting the measured optical spectra in the normal state (*20*, *21*), which are averages over all angles weighted by their Fermi velocity.

In Fig. 5, we calculate the real and imaginary parts of the pairing self-energy $\phi(\theta = 20°, \omega)$ from the deduced ε_N at 70 K (Fig. 4C) and at 35 K

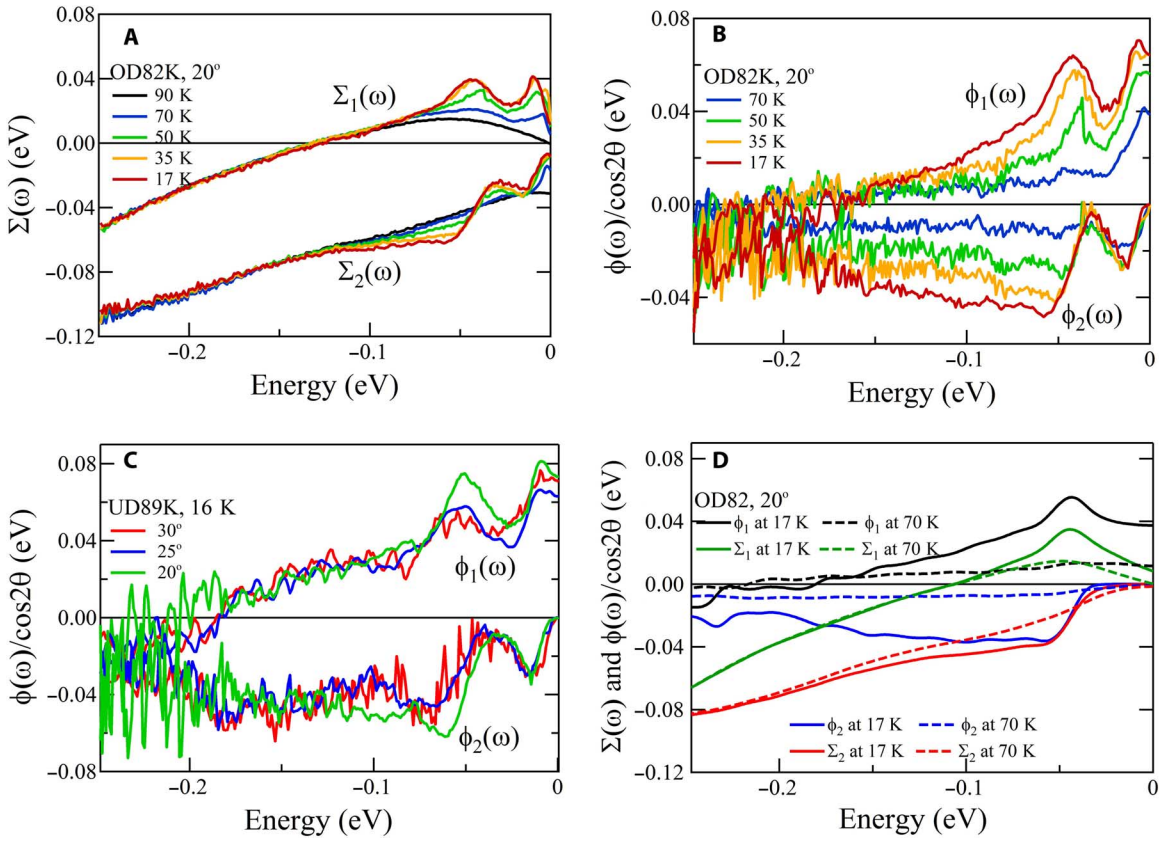

Fig. 3. Normal and pairing self-energies. (**A** and **B**) The evolution of the extracted normal self-energy (A) and the evolution of the pairing self-energy (B) as a function of temperature directly from the fits to the MDCs in OD82. The normal and pairing self-energies show superconducting gap–induced features at low energies up to about 3Δ and smoothly vary in energy thereafter up to a cutoff energy. (**C**) The pairing self-energies in UD89 at 16 K divided by cos(2θ). Determination of the pairing self-energy has acceptable signal-to-noise ratios up to about 0.2 eV only. The data fall together at the angles shown (up to an accuracy better than 10%) up to about 0.2 eV. (**D**) The self-energies smoothed over ±5 meV (as discussed in the text) and, after removing the impurity, induced features for OD82 at T = 17 K (solid lines) and T = 70 K (dashed lines).

(Fig. 4B) by using the Eliashberg equations and by assuming that $\varepsilon_P = \varepsilon_N$. The calculations (Fig. 5, solid lines) are directly compared with the extracted values (Fig. 5, circles and squares). Because $\phi \ll \Sigma$ near T_c, ε_N here is determined primarily by Σ. The measured ϕ determines the deduced ε_P using the Eliashberg equations. Therefore, the success of the comparison depends on both (i) $\varepsilon_N \approx \varepsilon_P$ near T_c, except for the small bump near 50 meV in ε_N, and (ii) the applicability and mutual consistency of the Eliashberg equations for the normal and pairing self-energies at a similar accuracy.

SALIENT POINTS OF THE EXPERIMENTAL RESULTS AND THEIR IMPLICATIONS

We extracted the electron self-energies in both pairing and full lattice symmetries directly from the ARPES data without adjustable parameters using the procedure described in section SII. We then used the integral equations, which are shown in section SIII, to numerically deduce both the pairing and the normal Eliashberg functions. No theoretical assumptions underlie our results, except that superconductivity is due to generalized BCS (Bardeen-Cooper-Schrieffer) pairing. We summarize here the principal conclusions of our data and analysis.

(A) The experimental results and their fits in Fig. 2 show that the imaginary part of the normal self-energy above is independent of **k** and linear in ω to a good approximation, as found earlier (*14*, *15*). The strange metal anomalies (such as the linear-in-T resistivity) and corresponding aspects in optical conductivity follow (*9*). The real and imaginary parts of both the normal and the pairing self-energies acquire superconductivity-induced features at low energy below T_c. The pairing self-energy near T_c is nearly a constant as a function of ω up to the upper cutoff and acquires the same superconductivity-induced features below T_c, as in the normal self-energy.

(B) In comparison with Fig. 4, one finds that, near T_c, $\varepsilon_P(\theta, \omega) \approx \varepsilon_N(\theta, \omega)$ to within the stated accuracy, except for the small bump near 50 meV in the latter. The part of these (dimensionless) quantities that is nearly a constant as a function of ω has the same magnitude as that of the normal state ε_N, and has a value of about 0.15 for UD89 and a consistently somewhat smaller value for OD82 up to the angle-dependent cutoff, which is about 0.2 eV at 20°, moving continuously to about 0.4 eV at 45°. Additional superconductivity-induced features in both functions are observed as temperature decreases well below T_c; within our accuracy, they have the same frequency dependence.

(C) Above T_c, $\varepsilon_N(\theta, \omega)$ consists of a low-energy bump at about 50 meV with a half-width of about 10 meV on top of a nearly constant part up to

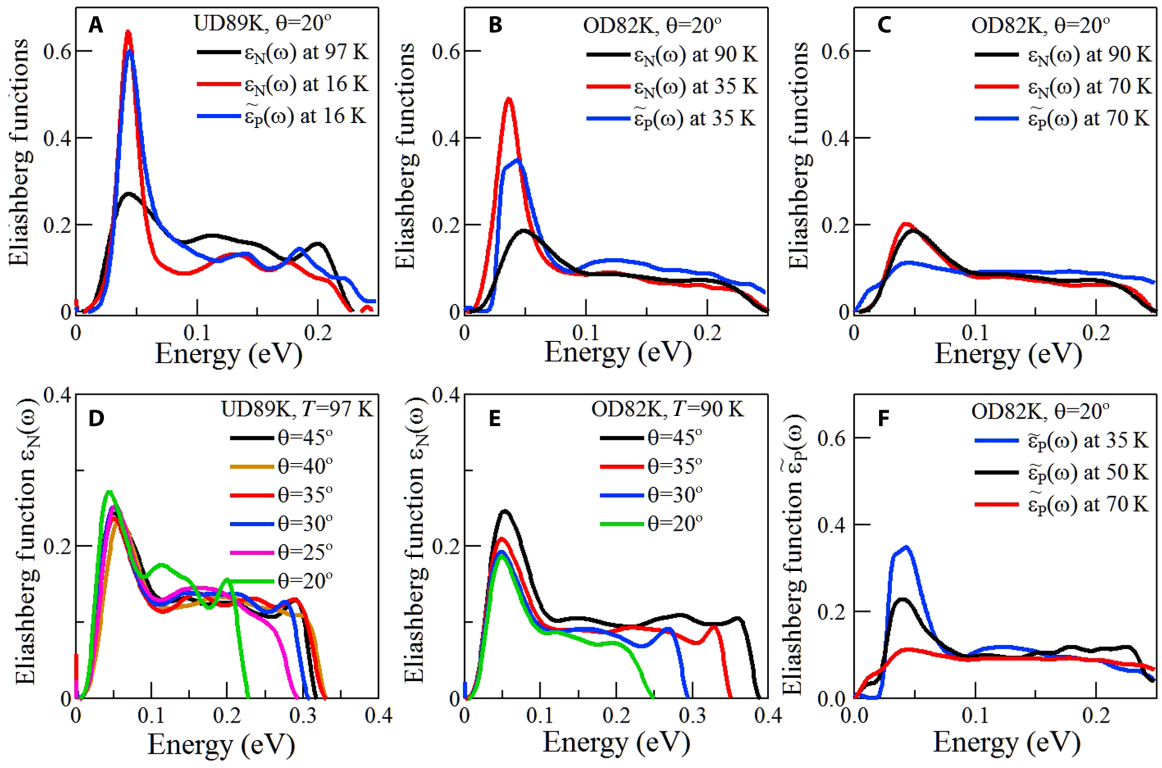

Fig. 4. Eliashberg functions: Normal [$\varepsilon_N(\theta, \omega)$] and scaled pairing [$\varepsilon_P(\theta, \omega) \equiv \varepsilon_P(\theta, \omega)/\cos(2\theta)$]. These are calculated using the solution for the Eliashberg equations from the measured self-energies. (**A**) and (**B**) compare $\varepsilon_P(20°, \omega)$ and $\varepsilon_N(20°, \omega)$ deep in the superconducting state for the two samples, and the latter also above T_c. At low temperatures, they are of the same accuracy over the whole frequency range, with a large superconductivity-induced enhanced low-energy peak. (**C**) Closer to T_c, the low-energy peak in $\varepsilon_P(\omega)$ disappears. This trend is shown more directly in (**F**). (**D**) and (**E**) give $\varepsilon_N(\theta, \omega)$ for T above T_c, showing the increase in cutoff energy with increasing θ. The gentle waviness in all of the results represents artifacts of the maximum entropy method for the solution of the Eliashberg equations.

the angle-dependent cutoff. $\varepsilon_P(\theta, \omega)$, which can be deduced only below T_c, has no low-energy bump near T_c. This means that coupling of fermions in the attractive d-wave channel to excitations that appear in the bump does not occur, but that coupling of fermions to such excitations in the s-wave channel does occur. On the other hand, the nearly constant part has a similar magnitude of coupling to fermions in both the s-wave channel and the d-wave channel.

(D) It is well understood (*22*, *23*) that d-wave pairing [that is, $\phi(\theta, \omega) \propto \cos 2\theta$] is favored only when fermions scatter dominantly over angles of $\pm \pi/2$. Together with point (C), this exposes the central paradox of d-wave superconductivity in cuprates: the fundamental physics of cuprates requires that the same fluctuations that dominantly scatter at angles $\pm \pi/2$ in the attractive channel lead to a nearly angle-independent repulsive scattering in the normal channel with the full symmetry of the lattice.

It is reasonable to assume that the bump in the normal state is due to optical phonons of apical oxygens, as has been suggested (*24*). In an interesting time-resolved conductivity experiment (*21*) at room temperature, the results were analyzed with fluctuations that could be divided into a peak at around 50 meV and a broad electronic continuum with a cutoff at about 0.4 eV; the bump has a relaxation rate that is much slower than the continuum, indicating independent sources for the two contributions. Our results for ε_N are consistent with these conclusions with the additional information (through ε_P) that the feature around 50 meV has no attractive coupling in the d-wave channel.

Determining T_c

One may wish to calculate T_c directly from the deduced Eliashberg functions. Such a check, however, is circular because the Eliashberg functions are obtained from the solution of equations whose linearized version yields T_c. Thus, if the complete information over the entire Brillouin zone were available, using the Eliashberg function near T_c back in the linearized Eliashberg equations would give the experimental T_c. Such an exercise may, however, be taken as a test of several of the steps in extracting the final results from the experiments and as a test of the extrapolations. Using the extrapolations for ε_P from the angles measured (so that their upper cutoff at other angles is also the same as the measured cutoff of ε_N) and extrapolating from the measured angles to all angles, the linearized Eliashberg equations for deductions, using $\xi(\mathbf{k})$ of Markiewicz *et al.* (*25*), indicate that $T_c \approx 135$ K for the UD89 sample and $T_c \approx 90$ K for the OD82 sample.

We can obtain estimates of the dimensionless coupling constants in the s-wave and d-wave channels by using their approximate expressions (*26*, *27*)

$$\begin{aligned} \lambda_s &\approx < \int_0^\infty d\omega \frac{2}{\omega} \varepsilon_N(\theta, \omega) >_\theta \\ \lambda_d &\approx < \int_0^\infty d\omega \frac{2}{\omega} \cos(2\theta) \varepsilon_P(\theta, \omega) >_\theta \end{aligned} \quad (1)$$

Using the result in Fig. 4C—that, near T_c, $\varepsilon_N(\theta, \omega) \approx \varepsilon_P(\theta, \omega) \approx 0.15$ from about T_c up to the cutoffs $\omega_c(\theta)$ and $\approx 0.15\omega/2T$ for $\omega \lesssim 2T$—yields

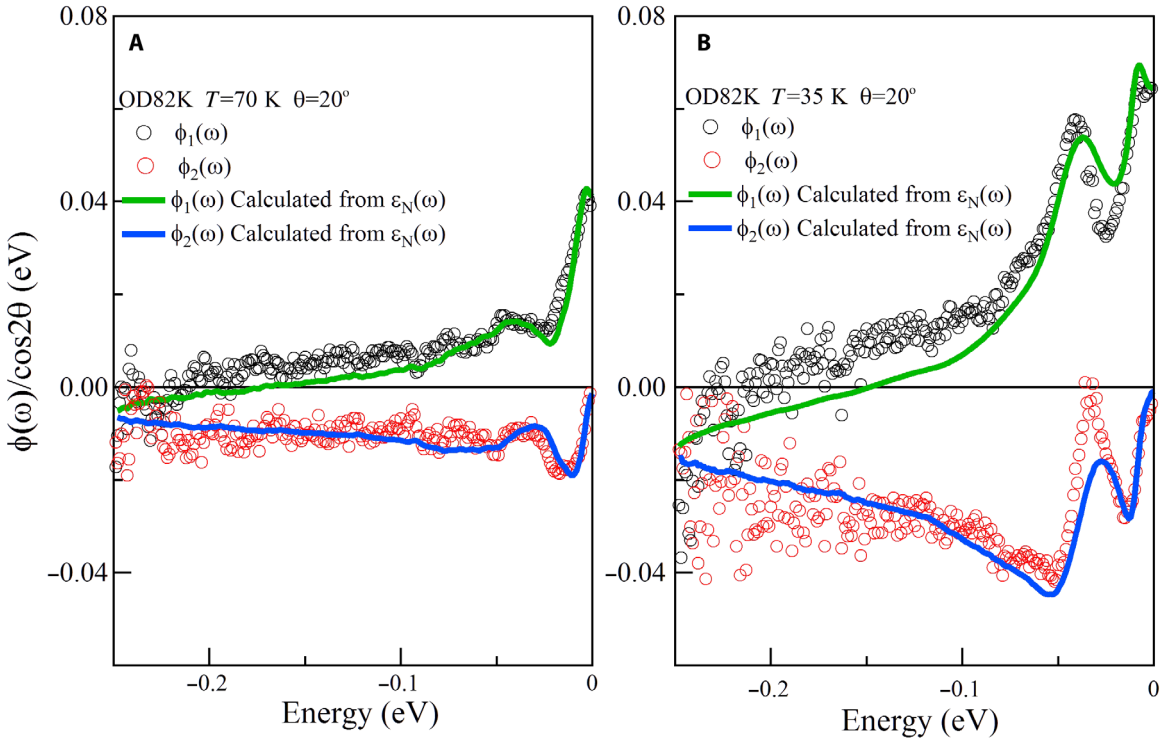

Fig. 5. Calculation of pairing self-energies assuming that $\varepsilon_P = \varepsilon_N$. (**A** and **B**) The experimentally deduced real and imaginary parts of self-energy (in absolute units) are compared with a calculation of the same quantity from the Eliashberg equations, assuming that $\varepsilon_P = \varepsilon_N$ for (A) $T = 70$ K and (B) $T = 35$ K in the OD82 sample. This agreement occurs only if the Eliashberg equations are applicable for the analysis of the data and for the relation of the two Eliashberg functions.

$\lambda \approx 2\lambda_d \approx 1.2$. In materials such as cuprates, where pair-breaking due to inelastic scattering is important, these parameters alone do not determine T_c (*27*). However, the deduced fluctuations provide an enhancement $0(\log(\omega_c/T_c))$ of the effective coupling constants, which are crucial factors in the proper determination of T_c for the kind of fluctuation spectrum deduced.

Brief comparison of cuprate models with the experimental results

The results in the literature for calculations starting with different physical ideas are compared to the experiments in section SIV. We summarize the comparisons here.

All calculations use adjustable parameters with which features of the experiments, such as T_c, may be reproduced. The comparison with experimental results must then be performed with respect to the momentum and frequency dependence of the pairing and normal self-energies and Eliashberg functions noted in principal conclusions (A) to (D).

(i) The calculations (*28*) using measurements (*29*) of antiferromagnetic spin fluctuations [in $(La_{2-x}Sr_x)CuO_4$ for $T/T_c \approx 0.25$] in the Eliashberg theory correctly give $\phi(\theta, \omega)$, consistent with $\propto \cos(2\theta)$. The calculations give a peak in $\phi(\theta, \omega)$, reproduced in fig. S3 at about 0.1 eV and nearly zero for the pairing self-energy beyond it. In Figs. 2 and 4 of Hong and Choi (*28*), $\Sigma(\omega, \theta)$ is not linear in ω and is strongly angle-dependent. To come to conclusions about the applicability of the theory, we should compare these results with the results in Fig. 3, which has a constant part in $\phi(\theta, \omega)/\cos(2\theta)$ up to the cutoff, a linear part in ω, and a nearly angle-independent part in $\Sigma(\omega, \theta)$ at all temperatures. Because no measurements are available at higher T, comparisons near T_c are not possible.

(ii) From the results of very extensive dynamical mean-field theory calculations on the Hubbard model (*30*, *31*), a value of the nearest-neighbor hopping parameter $t \approx 0.3$ eV is chosen to obtain nearly the right maximum value of $T_c \approx t/30$. Only angle-averaged self-energies are calculated with this technique. The calculations give peaks in the pairing self-energy (reproduced in fig. S4) at energies of about $0.2t$ and t (that is, between 0.06 and 0.3 eV), which sharply decrease to zero in between. The imaginary part of such a $\Sigma(\omega)$ [see Fig. 5 in Gull and Millis (*31*)] is constant beyond $\omega \approx 0.2t \approx 0.06$ eV, with a peak below this value. To come to conclusions about the inapplicability of the theory, we must compare these results with the experimental results in Fig. 3, which give, just below T_c, a linear part in ω self-energy and a nearly constant pairing self-energy up to the high-frequency cutoff.

(iii) The spectra of loop-current fluctuations are calculated as the quantum-critical fluctuations of the dissipative quantum *XY* model. It is proportional to $\tanh(\omega/2T)$ (*32*), with a high-frequency cutoff, which fits the deduced Eliashberg functions near T_c [except for the low-energy bump in $\varepsilon_N(\omega)$]. It leads to the well-known angle and frequency dependence of the measured normal self-energies. In Fig. 5, we have shown, in effect, that it also yields the measured pairing self-energy near T_c and well below T_c. In section IV, we recapitulate earlier results (*33*) about the momentum dependence of matrix elements coupling the fermions to fluctuations of the model so as to give both repulsion in the normal channel and attraction in the pairing channel

with the same frequency-dependent spectra. The physics behind the central paradox thereby follows.

MATERIALS AND METHODS

Optimally doped and slightly underdoped $Bi_2Sr_2CaCu2O_{8+\delta}$ (Bi2212) single crystals were grown by the traveling solvent floating zone method. The overdoped Bi2212 sample was prepared by annealing the optimally doped sample under an oxygen atmosphere. All of the samples were of high quality, exhibiting sharp superconducting transitions with a transition width of ~2 K.

Angle-resolved photoemission measurements were carried out in our vacuum ultraviolet laser-based angle-resolved photoemission system (*34*). The photon energy of the laser was 6.994 eV at a bandwidth of 0.26 meV, and the energy resolution of the electron energy analyzer (Scienta R4000) was set at 0.5 to 1 meV, giving rise to an overall energy resolution of ~1.0 meV. The angular resolution was about 0.3°, corresponding to a momentum resolution of ~0.004 $Å^{-1}$ at a photon energy of 6.994 eV. All samples were cleaved in situ and measured in vacuum with a base pressure better than 5×10^{-11} torr. More details about the sample and the experiments can be found in Zhang *et al.* (*6*, *35*) and He *et al.* (*7*).

SUPPLEMENTARY MATERIALS

Supplementary material for this article is available at http://advances.sciencemag.org/cgi/content/full/2/3/e1501329/DC1

SI. Extraction of normal and pairing self-energies from ARPES in the superconducting state

SI. 1. Single-particle spectral function

SI. 2. Procedure for extracting self-energy

SII. Correction of systematic errors and renormalization of ARPES data

SII. 1. Limits of the validity of results

SIII. Equations for self-energy

SIII. 1. Exact representation of self-energy

SIII. 2. Familiar Eliashberg integral equations for d-wave superconductors

SIV. Comparison of theories with experimental results

Fig. S1. Data corrections that are necessary because of systematic errors attributable to the movement of the sample with change in temperature.

Fig. S2. Exact representation of the normal and pairing self-energies.

Fig. S3. Imaginary part of the pairing self-energy at various angles across the Fermi surface calculated by Hong and Choi (*28*) from the spin-fluctuation spectra in $La_{2-x}Sr_xCuO_4$ measured by Vignolle *et al.* (*29*) at optimal doping.

Fig. S4. Imaginary part of the gap function for the Hubbard model calculated by Gull and Millis (*30*) for various dopings indicated in the plot.

References (*36*–*48*)

REFERENCES AND NOTES

1. W. L. McMillan, J. M. Rowell, Lead phonon spectrum calculated from superconducting density of states. *Phys. Rev. Lett.* **14**, 108–112 (1965).
2. G. Eliashberg, Interaction between electrons and lattice vibrations in a superconductor. *Sov. Phys. JETP* **11**, 696 (1960).
3. D. J. Scalapino, J. R. Schrieffer, J. W. Wilkins, Strong-coupling superconductivity. I. *Phys. Rev.* **148**, 263–279 (1966).
4. A. Damascelli, Z. Hussain, Z.-X. Shen, Angle-resolved photoemission studies of the cuprate superconductors. *Rev. Mod. Phys.* **75**, 473–541 (2003).
5. J. Campuzano, M. Norman, M. Randeria, Angle resolved photoemission in cuprate superconductors, vol. 2 of *The Physics of Superconductors* (Springer, New York, 1993), chap. 8.
6. W. Zhang, J. M. Bok, J. H. Yun, J. He, G. Liu, L. Zhao, H. Liu, J. Meng, X. Jia, Y. Peng, D. Mou, S. Liu, L. Yu, S. He, X. Dong, J. Zhang, J. S. Wen, Z. J. Xu, G. D. Gu, G. Wang, Y. Zhu, X. Wang, Q. Peng, Z. Wang, S. Zhang, F. Yang, C. Chen, Z. Xu, H.-Y. Choi, C. M. Varma, X. J. Zhou, Extraction of normal electron self-energy and pairing self-energy in the superconducting state of the $Bi_2Sr_2CaCu_2O_8$ superconductor via laser-based angle-resolved photoemission. *Phys. Rev. B* **85**, 064514 (2012).
7. J. He, W. Zhang, J. M. Bok, D. Mou, L. Zhao, Y. Peng, S. He, G. Liu, X. Dong, J. Zhang, J. S. Wen, Z. J. Xu, G. D. Gu, X. Wang, Q. Peng, Z. Wang, S. Zhang, F. Yang, C. Chen, Z. Xu, H.-Y. Choi, C. M. Varma, X. J. Zhou, Coexistence of two sharp-mode couplings and their unusual momentum dependence in the superconducting state of $Bi_2Sr_2CaCu_2O_{8+\delta}$ revealed by laser-based angle-resolved photoemission. *Phys. Rev. Lett.* **111**, 107005 (2013).
8. I. Vekhter, C. M. Varma, Proposal to determine the spectrum of pairing glue in high-temperature superconductors. *Phys. Rev. Lett.* **90**, 237003 (2003).
9. E. Abrahams, C. M. Varma, What angle-resolved photoemission experiments tell about the microscopic theory for high-temperature superconductors. *Proc. Natl. Acad. Sci. U.S.A.* **97**, 5714–5716 (2000).
10. L. Zhu, P. J. Hirschfeld, D. J. Scalapino, Elastic forward scattering in the cuprate superconducting state. *Phys. Rev. B* **70**, 214503 (2004).
11. S. H. Hong, J. M. Bok, W. Zhang, J. He, X. J. Zhou, C. M. Varma, H.-Y. Choi, Sharp low-energy feature in single-particle spectra due to forward scattering in *d*-wave cuprate superconductors. *Phys. Rev. Lett.* **113**, 057001 (2014).
12. P. B. Littlewood, C. M. Varma, Phenomenology of the superconductive state of a marginal Fermi liquid. *Phys. Rev. B Condens. Matter* **46**, 405–420 (1992).
13. A. W. Sandvik, D. J. Scalapino, N. E. Bickers, Effect of an electron-phonon interaction on the one-electron spectral weight of a *d*-wave superconductor. *Phys. Rev. B* **69**, 094523 (2004).
14. T. Valla, A. V. Fedorov, P. D. Johnson, Q. Li, G. D. Gu, N. Koshizuka, Temperature dependent scattering rates at the Fermi surface of optimally doped $Bi_2Sr_2CaCu_2O_{8+\delta}$. *Phys. Rev. Lett.* **85**, 828–831 (2000).
15. A. Kaminski, H. M. Fretwell, M. R. Norman, M. Randeria, S. Rosenkranz, U. Chatterjee, J. C. Campuzano, J. Mesot, T. Sato, T. Takahashi, T. Terashima, M. Takano, K. Kadowaki, Z. Z. Li, H. Raffy, Momentum anisotropy of the scattering rate in cuprate superconductors. *Phys. Rev. B* **71**, 014517 (2005).
16. J. M. Bok, J. H. Yun, H.-Y. Choi, W. Zhang, X. J. Zhou, C. M. Varma, Momentum dependence of the single-particle self-energy and fluctuation spectrum of slightly underdoped $Bi_2Sr_2CaCu_2O_{8+\delta}$ from high-resolution laser angle-resolved photoemission. *Phys. Rev. B* **81**, 174516 (2010).
17. A. A. Kordyuk, S. V. Borisenko, M. Knupfer, J. Fink, Measuring the gap in angle-resolved photoemission experiments on cuprates. *Phys. Rev. B* **67**, 064504 (2003).
18. W. H. Press, S. A. Teukolsky, W. T. Vetterling, B. P. Flannery, *Numerical Recipes* (Cambridge Univ. Press, New York, 2002), 1002 pp.
19. E. Schachinger, J. P. Carbotte, Finite band inversion of angular-resolved photoemission in $Bi_2Sr_2CaCu_2O_{8+\delta}$ and comparison with optics. *Phys. Rev. B* **77**, 094524 (2008).
20. E. van Heumen, E. Muhlethaler, A. B. Kuzmenko, H. Eisaki, W. Meevasana, M. Greven, D. van der Marel, Optical determination of the relation between the electron-boson coupling function and the critical temperature in high-T_c cuprates. *Phys. Rev. B* **79**, 184512 (2009).
21. S. Dal Conte, C. Giannetti, G. Coslovich, F. Cilento, D. Bossini, T. Abebaw, F. Banfi, G. Ferrini, H. Eisaki, M. Greven, A. Damascelli, D. van der Marel, F. Parmigiani, Disentangling the electronic and phononic glue in a high-T_c superconductor. *Science* **335**, 1600–1603 (2012).
22. K. Miyake, S. Schmitt-Rink, C. M. Varma, Spin-fluctuation-mediated even-parity pairing in heavy-fermion superconductors. *Phys. Rev. B Condens. Matter* **34**, 6554–6556 (1986).
23. C. M. Varma, Considerations on the mechanisms and transition temperatures of superconductivity induced by electronic fluctuations. *Rep. Prog. Phys.* **75**, 052501 (2012).
24. A. Lanzara, P. V. Bogdanov, X. J. Zhou, S. A. Kellar, D. L. Feng, E. D. Lu, T. Yoshida, H. Eisaki, A. Fujimori, K. Kishio, J.-I. Shimoyama, T. Noda, S. Uchida, Z. Hussain, Z.-X. Shen, Evidence for ubiquitous strong electron–phonon coupling in high-temperature superconductors. *Nature* **412**, 510–514 (2001).
25. R. S. Markiewicz, S. Sahrakorpi, M. Lindroos, H. Lin, A. Bansil, One-band tight-binding model parameterization of the high-T_c cuprates including the effect of k_z dispersion. *Phys. Rev. B* **72**, 054519 (2005).
26. W. L. McMillan, Transition temperature of strong-coupled superconductors. *Phys. Rev.* **167**, 331–344 (1968).
27. A. J. Millis, S. Sachdev, C. M. Varma, Inelastic scattering and pair breaking in anisotropic and isotropic superconductors. *Phys. Rev. B Condens. Matter* **37**, 4975–4986 (1988).
28. S. H. Hong, H.-Y. Choi, Angle and frequency dependence of self-energy from spin fluctuations mediated d-wave pairing for high temperature superconductors. *J. Phys. Condens. Matter* **25**, 365702 (2013).
29. B. Vignolle, S. M. Hayden, D. F. McMorrow, H. M. Rønnow, B. Lake, C. D. Frost, T. G. Perring, Two energy scales in the spin excitations of the high-temperature superconductor $La_{2-x}Sr_xCuO_4$. *Nat. Phys.* **3**, 163–167 (2007).
30. E. Gull, A. J. Millis, Pairing glue in the two-dimensional Hubbard model. *Phys. Rev. B* **90**, 041110 (2014).
31. E. Gull, A. J. Millis, Quasiparticle properties of the superconducting state of the two-dimensional Hubbard model. *Phys. Rev. B* **91**, 085116 (2015).
32. L. Zhu, Y. Chen, C. M. Varma, Local quantum criticality in the two-dimensional dissipative quantum *XY* model. *Phys. Rev. B* **91**, 205129 (2015).
33. V. Aji, A. Shekhter, C. M. Varma, Theory of the coupling of quantum-critical fluctuations to fermions and *d*-wave superconductivity in cuprates. *Phys. Rev. B* **81**, 064515 (2010).

34. G. Liu, G. Wang, Y. Zhu, H. Zhang, G. Zhang, X. Wang, Y. Zhou, W. Zhang, H. Liu, L. Zhao, J. Meng, X. Dong, C. Chen, Z. Xu, X. J. Zhou, Development of a vacuum ultraviolet laser-based angle-resolved photoemission system with a superhigh energy resolution better than 1 meV. *Rev. Sci. Instrum.* **79**, 023105 (2008).
35. W. Zhang, G. Liu, L. Zhao, H. Liu, J. Meng, X. Dong, W. Lu, J. S. Wen, Z. J. Xu, G. D. Gu, T. Sasagawa, G. Wang, Y. Zhu, H. Zhang, Y. Zhou, X. Wang, Z. Zhao, C. Chen, Z. Xu, X. J. Zhou, Identification of a new form of electron coupling in the $Bi_2Sr_2CaCu_2O_8$ superconductor by laser-based angle-resolved photoemission spectroscopy. *Phys. Rev. Lett.* **100**, 107002 (2008).
36. J. H. Yun, J. M. Bok, H.-Y. Choi, W. Zhang, X. J. Zhou, C. M. Varma, Analysis of laser angle-resolved photoemission spectra of $Ba_2Sr_2CaCu_2O_{8+\delta}$ in the superconducting state: Angle-resolved self-energy and the fluctuation spectrum. *Phys. Rev. B* **84**, 104521 (2011).
37. A. A. Galkin, A. I. D'yachenko, V. M. Svistunov Determination of the energy gap parameter and of the electron-phonon interaction in superconductors from the tunnel data. *Zh. Eksp. Teor. Fiz.* **66**, 2262–2268 (1974).
38. P. Nozieres, *Theory of Interacting Fermi Systems* (Benjamin, New York, 1960).
39. A. A. Abrikosov, L. Gorkov, I. Dzyaloshinski, *Methods of Quantum Field Theory in Statistical Physics* (Prentice Hall Inc., New Jersey, 1963).
40. D. J. Scalapino, E. Loh Jr., J. E. Hirsch, *d*-wave pairing near a spin-density-wave instability. *Phys. Rev. B Condens. Matter* **34**, 8190–8192 (1986).
41. S. Nishiyama, K. Miyake, C. M. Varma Superconducting transition temperatures for spin-fluctuation superconductivity: Application to heavy-fermion compounds. *Phys. Rev. B* **88**, 014510 (2013).
42. S. S. Kancharla, B. Kyung, D. Sénéchal, M. Civelli, M. Capone, G. Kotliar, A.-M. S. Tremblay, Anomalous superconductivity and its competition with antiferromagnetism in doped Mott insulators. *Phys. Rev. B* **77**, 184516 (2008).
43. P. Bourges, Y. Sidis, Novel magnetic order in the pseudogap state of high-copper oxides superconductors. *C. R. Phys.* **12**, 461–479 (2011).
44. M. E. Simon, C. M. Varma, Detection and implications of a time-reversal breaking state in underdoped cuprates. *Phys. Rev. Lett.* **89**, 247003 (2002).
45. C. M. Varma, Non-Fermi-liquid states and pairing instability of a general model of copper oxide metals. *Phys. Rev. B* **55**, 14554–14580 (1997).
46. V. Aji, C. M. Varma, Quantum criticality in dissipative quantum two-dimensional ***XY*** and Ashkin-Teller models: Application to the cuprates. *Phys. Rev. B* **79**, 184501 (2009).
47. V. Aji, C. M. Varma Topological excitations near the local critical point in the dissipative two-dimensional ***XY*** model. *Phys. Rev. B* **82**, 174501 (2010).
48. C. M. Varma, P. B. Littlewood, S. Schmitt-Rink, E. Abrahams, A. E. Ruckenstein, Phenomenology of the normal state of Cu-O high-temperature superconductors. *Phys. Rev. Lett.* **63**, 1996–1999 (1989).

Acknowledgments: C.M.V. thanks E. Abrahams for a discussion of the exact relation of irreducible vertices to self-energy. **Funding:** H.-Y.C. was supported by the National Research Foundation of Korea (grant NRF-2013R1A1A2061704). X.J.Z. received financial support from the National Natural Science Foundation of China (grants 11190022 and 11334010), the Ministry of Science and Technology of China (973 Programs 2011CB921703 and 2011CBA00110), and the Strategic Priority Research Program (B) of the Chinese Academy of Sciences (grant XDB07020300). C.M.V. was partially supported by NSF grant DMR 1206298. **Author contributions:** The project was conceived by C.M.V., X.J.Z., and H.-Y.C. The measurements were performed by W.Z. and J.H. under the supervision of X.J.Z. The experimental data were analyzed by J.H., W.Z., Y.Z., L.Y., and J.M.B. under the supervision of H.-Y.C., C.M.V., and X.J.Z. The extraction of self-energy and Eliashberg functions and the theoretical modeling were carried out by J.M.B. and J.J.B., whereas the figures were plotted by J.M.B., W.Z., and J.H., under the supervision of H.-Y.C., C.M.V., and X.J.Z. The manuscript was written by C.M.V., H.-Y.C., and X.J.Z. All authors participated in the discussion of the results and in the writing of the paper. **Competing interests:** The authors declare that they have no competing interests. **Data and materials availability:** All data needed to evaluate the conclusions in the paper are present in the paper and/or the Supplementary Materials. Additional data related to this paper may be requested from the authors.

Submitted 24 September 2015
Accepted 5 January 2016
Published 4 March 2016
10.1126/sciadv.1501329

Citation: J. M. Bok, J. J. Bae, H.-Y. Choi, C. M. Varma, W. Zhang, J. He, Y. Zhang, L. Yu, X. J. Zhou, Quantitative determination of pairing interactions for high-temperature superconductivity in cuprates. *Sci. Adv.* **2**, e1501329 (2016).